Biochemistry

pubs.acs.org/biochemistry Article

Delocalization-Assisted Transport through Nucleic Acids in Molecular Junctions

Jesús Valdiviezo,[#] Caleb Clever,[#] Edward Beall, Alexander Pearse, Yookyung Bae, Peng Zhang,* Catalina Achim, David N. Beratan,* and David H. Waldeck*

Cite This: *Biochemistry* 2021, 60, 1368−1378 Read Online

ACCESS | Metrics & More | Article Recommendations | Supporting Information

ABSTRACT: The flow of charge through molecules is central to the function of supramolecular machines, and charge transport in nucleic acids is implicated in molecular signaling and DNA repair. We examine the transport of electrons through nucleic acids to understand the interplay of resonant and nonresonant charge carrier transport mechanisms. This study reports STM break junction measurements of peptide nucleic acids (PNAs) with a G-block structure and contrasts the findings with previous results for DNA duplexes. The conductance of G-block PNA duplexes is much higher than that of the corresponding DNA duplexes of the same sequence; however, they do not display the strong even−odd dependence conductance oscillations found in G-block DNA. Theoretical analysis finds that the conductance oscillation magnitude in PNA is suppressed because of the increased level of electronic coupling interaction between G-blocks in PNA and the stronger PNA−electrode interaction compared to that in DNA duplexes. The strong interactions in the G-block PNA duplexes produce molecular conductances as high as 3% G_0, where G_0 is the quantum of conductance, for 5 nm duplexes.

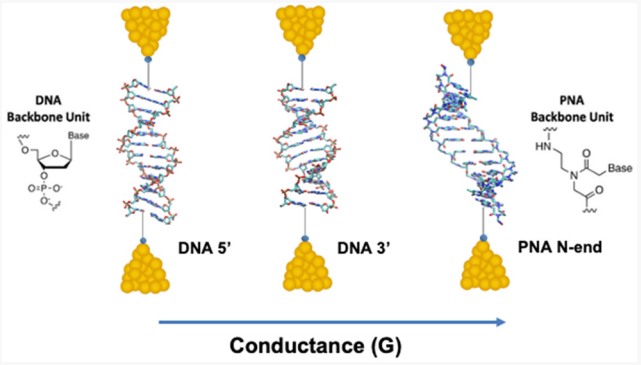

The transport of charge through nucleic acids[1−12] can proceed by tunneling, resonant, near-resonant, or incoherent pathways that are sensitive to the macromolecular structure and its environment.[13−16] Until recently, the transport of charge through nucleic acids was believed to proceed by coherent tunneling at shorter distances and incoherent (multistep) hopping at longer distances.[11,17−19] However, recent studies found that neither the coherent nor the incoherent pictures are adequate to describe the transport at short to intermediate distances.[20−22] For example, the single-molecule conductances measured for deoxyribonucleic acid (DNA) duplexes with alternating cytosine (C) and guanine (G) bases, namely -$(GC)_n$- with n ranging from 3 to 8, were compared to those for duplexes of the same length with the G and C bases separated into blocks, i.e., -G_nC_n-.[21] The conductance of the -$(GC)_n$- duplex decreases linearly with n, while the conductance of the -G_nC_n- (G-block) duplex oscillates with n. The linear decrease in the conductance of $(GC)_n$ is consistent with an incoherent charge transport mechanism. The G-block conductance oscillations suggest extended carrier delocalization (coherence) over adjacent G-blocks.[23]

The strong sequence dependent conductance found for DNA[7] charge transfer[24−28] indicate sequence-dependent delocalization characteristics. Indeed, the more rapid exponential decrease in electrical conductance in AT duplexes compared to that in GC duplexes is well documented.[29] Less well understood is the influence of cross-strand couplings on the strength and mechanism of nucleic acid charge transfer and transport.[30] For example, positioning the molecule−electrode linker groups and the G-blocks on the 3′ termini of the DNA duplexes causes an order of magnitude increase in the single-molecule conductance compared to that of duplexes with the electrode−molecule linkers and G-blocks on the 5′ termini. This conductance enhancement of the 3′-anchored G-block duplexes was explained by the stronger cross-strand G-to-G coupling between G-blocks accessed in the middle of the 3′−3′ structure, compared to the corresponding cross-strand coupling in the 5′−5′ chains.[30] Because the G-blocks mediate charge flow,[24] the cross-strand block-to-block coupling is critical.[31] Indeed, the G-to-G cross-strand coupling is estimated to be 2−3 times larger in the 3′-anchored duplexes than in the 5′-anchored species.[32] The smaller cross-strand coupling in the 5′-anchored duplexes was suggested to be responsible for the enhanced even-odd conductance oscillations that were observed experimentally.[30]

Received: January 26, 2021
Revised: April 5, 2021
Published: April 19, 2021

https://doi.org/10.1021/acs.biochem.1c00072
Biochemistry 2021, 60, 1368−1378

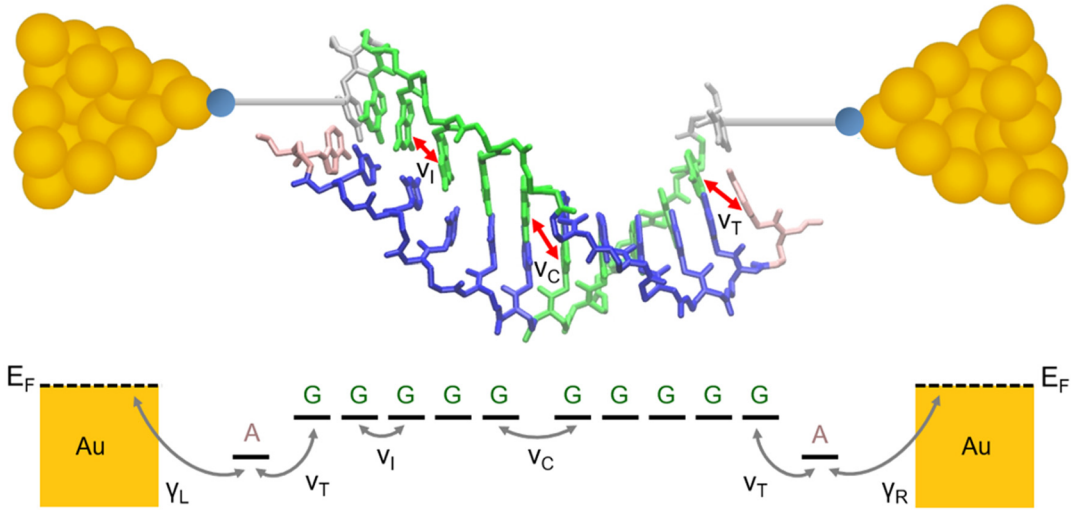

Figure 1. Orientations of opposing termini (top) for the N-linked PNA for n = 5. The sequence shown is TG_5C_5A, and each color represents a different nucleotide. The duplexes are anchored to gold electrodes via amine modifications on the terminal thymine nucleobase. The arrows indicate the nucleobases considered for the GC-GC intrastrand (V_I), GC-GC cross-strand (V_C), and terminal AT-GC (V_T) electronic coupling calculations. One-dimensional model used in this work (bottom). E_F is the Fermi level of the gold electrode. γ_L and γ_R are the molecule−lead electronic couplings. V_I, V_C, and V_T are the nucleobase electronic couplings described above.

Comparing the molecular conductance through aminoethylglycine peptide nucleic acid (PNA) and DNA duplexes with the same base sequences can help to reveal the structural origins of the molecular conductances.[33−36] PNA and DNA duplexes that have the same number of bases and the same sequence, but a different backbone structure, can display conductances that differ by 10−20-fold.[36] These conductance differences were explained as arising from differences in the occurrence of strongly coupled nucleobases, as well as by differences of energy level broadenings. Indeed, energy level broadening can produce mechanisms that are neither purely coherent nor incoherent. The "flickering resonance" mechanism[37] relies on accessing conformations through molecular fluctuations that can support coherent transport during the persistence time of the quasi-degenerate energy configurations. The studies reported here describe the single-molecule conductance of G-block PNA duplexes for five different lengths (n = 3−7) and compare the conductances to those measured in G-block DNA duplexes reported previously.[30] This study explores how changes in backbone chemistry influence the conductance values and the relative contributions of coherent and incoherent transport mechanisms.

The structure of N-linked PNA is shown in Figure 1. An amine-modified thymine nucleobase is positioned at the N-terminus of the self-complementary G-block PNA oligomer; Watson−Crick hybridization of the PNA oligomer leads to a PNA duplex that has a palindromic sequence with amine-modified thymines on both ends of the duplex. Electronic coupling occurs between the electrode and the amine-modified thymine at the N-terminus of one strand of the duplex; the modified thymine at the N-terminus of the complementary strand interacts with the STM break junction tip (N-to-N transport). The N-terminus of PNA is analogous to the 5′ terminus of DNA.[38] The conductance measured for the G-block PNA duplexes is as much as 20 times larger than that measured for the analogous G-block DNA duplexes, and the even−odd conductance oscillations are found to be less pronounced in PNA.

The enhanced conductance of PNA duplexes, found in earlier comparisons between DNA and PNA homoduplexes, was attributed to the greater backbone structural flexibility in PNA.[36] The study presented here shows that the conductance of G-block PNA is larger than in G-block DNA; however, the G-block duplexes of DNA and PNA appear to have similar structural flexibility (*vide infra*). Nevertheless, the theoretical analysis suggests that the structural changes associated with the different nucleic acid backbones affect the electronic couplings through the π-stack and the nucleic acid−electrode interactions, producing stronger electrode−molecule coupling for PNA than for DNA. That is, the electronic coupling interactions near the chain ends (γ_L, γ_R, and V_T, indicated in the lower panel of Figure 1) are much larger for PNA duplexes than for DNA duplexes. The measured conductance value trends for the three duplex types and the magnitude of the even−odd conductance oscillations are rationalized using an orbital model to describe the mediating states (*vide infra*).

EXPERIMENTAL AND COMPUTATIONAL METHODS

Conductance Measurements. Single-molecule conductances were measured for PNA duplexes of different lengths tethered at the N-chain ends. A diffuse duplex monolayer was formed on a gold substrate by spontaneous adsorption from a Tris-EDTA buffer solution of a nucleic acid with amine linkers attached to the terminal thymine nucleobases. The electrical conductance of nucleic acid duplexes trapped in a junction between the STM tip and the gold substrate was measured using an ac-modulated scanning tunneling microscope break junction (STM-BJ) method.[39,40] This experiment drives the STM tip to the surface of the gold substrate and then withdraws it, allowing molecular junctions to form between the substrate and tip. During each tip withdrawal, a triangular voltage waveform is applied between the STM tip and the substrate and a set of current−time profiles are collected. Figure 2 shows an example of a single time trajectory for an STM−PNA−substrate junction, in which the PNA is a sequence of 12 nucleobase pairs. In this experiment, the

https://doi.org/10.1021/acs.biochem.1c00072
Biochemistry 2021, 60, 1368−1378

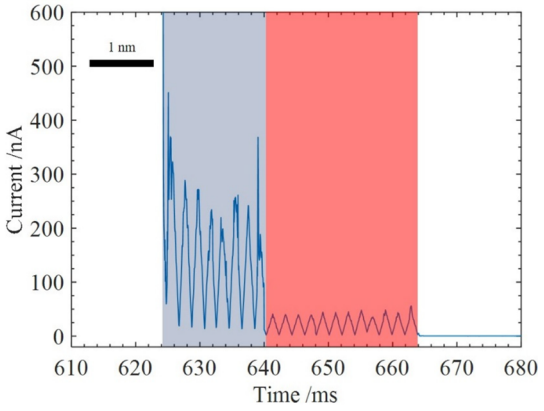

Figure 2. Example current−time $I(t)$ trajectory of a PNA 12-mer G-block molecular junction. Each triangular period is 2 ms in duration; the STM tip retracts by 0.2 nm during each current response period, and the bar shown at the top left gives the length scale. The initial region (blue) corresponds to the high-conductance mode, while the later region (red) is the lower mode. Note that the junction persists for ∼4 nm, which corresponds to the full length of the PNA molecule.

STM tip is retracted at a rate of 0.1 nm/ms as the bias voltage is modulated with a 2 ms period. The retraction rate was chosen to balance the stability and duration of the molecular junctions. The total length of the trajectory in Figure 2 is ∼4 nm. Note the sharp change in the current levels near the 640 ms time point. This change is indicative of two distinct junction geometries, and they are described extensively in previous reports.[29,36,40] Conductance measurements on duplex DNA were performed in mesitylene, and values were compared to earlier measurements in buffer solutions.[30] Good agreement among the measurements was found, suggesting no significant changes in the conformations of the nucleic acids. For this reason, and for reasons of experimental convenience, conductances were measured in a mesitylene solution. Fitting these current−time profiles using a circuit model allows molecular conductance G to be extracted from the data, and these values are used to build conductance histograms (see the Supporting Information).[41] Note that background conductance histograms were also measured in experiments without PNA molecules present. It has been reported that molecular junctions of mesitylene produce conductance values of approximately 0.03 and 0.1 G/G_0.[42,43] However, the length of these junctions is very short, ∼0.2 nm, which corresponds to a single voltage modulation period in our measurement (see Figure 2), and it is rejected by our criterion that the molecular junction must persist for at least four voltage modulation periods at a consistent current level to indicate a nucleic acid molecular junction. Therefore, any mesitylene conductances that are recorded would be significantly less prevalent than the nucleic acid junctions, as is shown by the control experiments (see the Supporting Information for more details).

Molecular Dynamics Simulations. Nucleic acid conformations were sampled using classical molecular dynamics (MD) simulations, and the structures provide a starting point for computing the energies of specific base orbitals and their electronic coupling interactions. Initial B-DNA structures were obtained using the Avogadro DNA builder tool,[44] and PNA duplexes were generated with the Schrödinger Maestro molecular modeling software,[45] starting from a right-handed PNA crystal structure with a heterogeneous sequence (Protein Data Bank entry 3MBS).[46] The CHARMM36 force field DNA parameters,[47] and the recently developed PNA parameters,[48] were used (the new PNA force field produces structural ensembles that are consistent with those found using other force fields in earlier studies).[36] The structures were solvated in

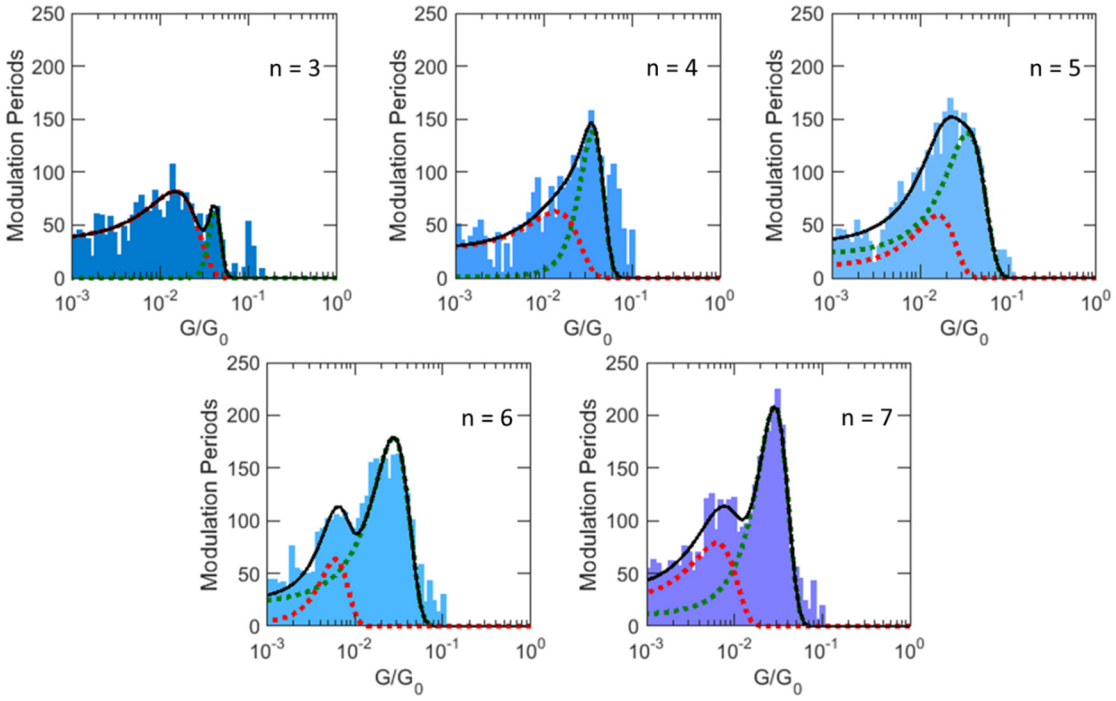

Figure 3. Conductance histograms for the N-to-N linked PNA for n = 3−7. The black curve is a sum of two Gaussian functions. The dotted red and green curves are the individual Gaussians for the low and high-conductance modes, respectively. The y-axis shows the number of modulation periods measured.

https://doi.org/10.1021/acs.biochem.1c00072
Biochemistry 2021, 60, 1368−1378

a TIP3P water box[49] that extended at least 15.0 Å from each atom. A distance constraint was added between the terminal base pairs to prevent fraying.[50] NAMD version 2.11[51] was used to run the MD simulations. After energy minimization and equilibration, the solvated structures were subjected to 100 ns of MD simulation at 300 K and 1 atm pressure. Snapshots for each system were saved every 33 ps (3000 coordinate snapshots in all). A detailed description of the procedure is found in the Supporting Information.

Electronic Coupling and Site Energy Analysis. For each MD snapshot, the nucleobase HOMO energies and nearest-neighbor cross-strand (V_C), intrastrand (V_I), and terminal AT-GC (V_T) couplings (Figure 1) were computed from the Fock matrix using the block diagonalization method;[52] the Fock matrix was obtained at the INDO/S level[53] from the CNDO program.[54] The INDO/S method gives a good description of charge transfer parameters in organic π-stacks at a reasonable computational cost.[55] Electronic couplings were computed in the two-state approximation. Only the nucleobases were included in the computation of orbital energies and electronic couplings, denoted as *in vacuo* (solvent and backbone atoms were removed, and dangling bonds were capped with hydrogens). The explicit treatment of backbone and solvent as classical point charges (QM/MM scheme) has been reported to have a small influence on the HOMO energy mean values,[56] and in sequences with longer bridges, as in this study, the rate constants for hole transfer calculated using a QM/MM formalism and *in vacuo* approaches are similar.[57] It has also been shown that electronic couplings calculated using the QM/MM formalism are similar to the *in vacuo* results,[56,57] so we used the *in vacuo* results in the analysis described here. The methods used here were shown to provide reliable estimates of the electronic couplings in DNA.[32,33]

A cross-strand coupling via the superexchange guanine-cytosine-guanine pathway was also calculated for snapshots taken every 5 ns, using only the four nucleobases in the cross-strand region. A density functional theory approach was selected to describe the hydrogen bonding interactions between nucleobases,[58] which are relevant for the superexchange pathway. The Kohn−Sham matrix obtained with the M11 functional[59] and the ma-def2-TZVPP basis set[60] as implemented in Gaussian 16[61] was used to compute the associated electronic couplings.

RESULTS AND DISCUSSION

PNA Duplex Conductance. Conductance histograms for the N-to-N linked PNA duplexes with the TG_nC_nA sequence (n = 3−7) are shown in Figure 3, and the most probable conductance for each mode is reported in Table 1. All conductance histograms have two peaks, similar to the histograms reported for other PNA duplexes.[36] The multiple peaks in the molecular conductance histograms were assigned to distinct "conductance modes" that can arise from different binding modes of the linkers and the gold atoms of the surface, specifically the number of gold atoms bonded to the linker, or from different conformations of the molecular junctions.[62,63] The contribution of higher-conductance modes increases with duplex length. This correlation is consistent with the experimental observation that shorter duplexes, which have lower thermal stability, have shorter average residence times in the junction.[29] Thus, the increased statistical weighting of the high-conductance mode likely indicates an increased fraction of more stable π-stacked duplexes in the junction, arising from the presence of stronger π-overlap between the GC pairs that make the structure more rigid. A more detailed discussion of the different "conductance modes", as well as transitions between them (see Figure 2) and how they are distinguished by the length of time a molecule remains in the junction, is provided in refs 29 and 40.

Table 1. Average Conductance Values of the Highest Observable Mode, G, and the Standard Deviation, σ_G, from the Gaussian Fits for the N-Linker PNA Duplexes for Lengths n = 3−7

n	G/G_0 ($\times 10^{-2}$)	σ_G/G_0 ($\times 10^{-2}$)
3	4.2	0.6
4	3.6	1.0
5	3.5	1.8
6	2.8	1.4
7	2.9	1.2

Although both modes are shown in Figure 3, the analysis and discussion focus on the highest-conductance mode to draw comparisons with the earlier G-block DNA studies that focused on the highest-conductance modes. In some instances, most notably for n = 4, a shoulder or second peak appears at twice the conductance value of the most probable peak for a given conductance mode. This feature was analyzed previously, as well, and is attributed to two or more molecules forming in a molecular junction.[29,40] In contrast to earlier STM break junction studies of PNA in which the conductance was well below 10^{-3} G_0, the G-block duplexes studied here have conductances that are a few percent of G_0. Measurements at these higher conductances created the need to distinguish molecular signals from background signals arising from (sub)oxide formation on the substrate that appear at ∼0.1 G_0. The measurement protocols and control experiments used to distinguish the two signals are described in the Supporting Information. The conductance shoulders of the histograms in Figure 3 and the (sub)oxide signal were excluded from the Gaussian fitting.

The average single-molecule conductance for the high-conductance mode shows a modest decrease as the duplex length increases (see Table 1). The influence of the background signal on the measurements is negligible for the n = 4−7 duplexes but may contribute to the n = 3 measurement, because fewer molecular junctions were sampled in this case (given the decreased residence time of the duplex in the junction). To account for these signal-to-noise constraints, more extensive background measurements were performed, and the peak at ∼0.1 G_0 was excluded from the analysis (see the Supporting Information). Note that Table S1 provides a listing of the conductances and standard deviations for the lower-conductance mode.

The conductances of the -(G_nC_n)- PNA duplexes show a nearly monotonic, albeit weak, decrease as n increases. Figure 4 plots these PNA data and the conductance data for 3′ DNA G-blocks and 5′ DNA G-blocks. We measured molecular conductances for n = 3−5 G-blocks of 3′ and 5′ DNA duplexes (see the Supporting Information) and found good agreement with the values reported earlier by Tao and co-workers.[21,30] Both of these data sets, the sets reported here and those reported by Tao, are plotted in Figure 4. These data highlight the significant difference in the average conductance

https://doi.org/10.1021/acs.biochem.1c00072
Biochemistry 2021, 60, 1368−1378

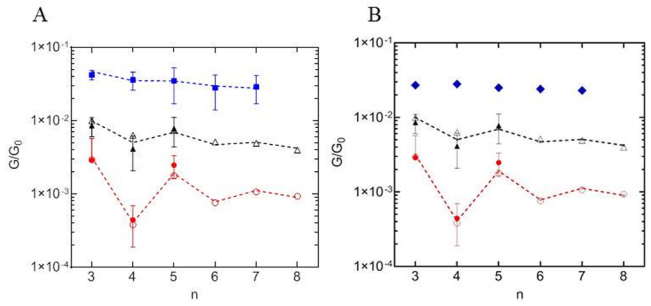

Figure 4. (A) Average conductance for the N-linker PNA (blue squares) with data for 3′-linker DNA (black triangles) and 5′-linker DNA (red circles). The empty symbols are from a previous study[30] and the filled symbols are from this study. Error bars are shown for the duplexes studied here representing a single standard deviation of the fitted Gaussian function for the highest observable mode. The negative component of the error for the 5′-linker DNA n = 3 data point has been excluded for the sake of clarity. The lines in the plot connect the best fit conductances found using the Büttiker double barrier model (see the Supporting Information). (B) Alternate analysis in which the PNA conductance values were assigned to the mean conductance value of the histogram, to show the increased PNA conduction in a model-independent manner.

for the three duplex types, as well as the decreasing prominence of the conductance variations with even and odd G-block lengths in the three duplexes (see the Supporting Information for plots showing the lower-conductance modes).

Theoretical Analysis of DNA and PNA Structures and Electronic Properties. Molecular dynamics simulations of PNA and DNA duplexes -(G_5C_5)- were run for 100 ns. This time range allows sampling of the internucleobase fluctuations and a subset of duplex conformational changes.[33] Analysis of these structural data indicates that the root-mean-square deviations (RMSDs) for the structural fluctuations of PNA duplexes are comparable to those of the DNA duplexes. The duplex RMSD value from its average structure calculated with VMD[64] is 1.3 ± 0.3 Å for N-linked PNA, 1.4 ± 0.4 Å for 3′-linked DNA, and 1.5 ± 0.4 Å for 5′-linked DNA. The small difference in RMSD values suggests that the PNA duplexes are slightly more rigid than the corresponding DNA structures (see Figures S5 and S6). This result is the opposite of results that were found earlier for PNA and DNA duplexes with a mixed nucleobase sequence. (For mixed sequences, the PNA duplexes were found to be more flexible than the DNA duplexes.[33]) This finding indicates that the relative structural flexibility of the nucleic acids is sequence-dependent. The larger overlap between nucleobases in the PNA G-blocks leads to stronger $\pi-\pi$ interactions and decreased flexibility as compared to those of mixed sequence PNA duplexes.[65]

MD snapshots were used to calculate HOMO energy fluctuations for each base pair in the duplexes (at the INDO/S level). The HOMO energy fluctuations and standard deviations of each base pair are listed in Table 2 for the n = 5 length, which is illustrated in Figure 1, for the case of PNA. The similar HOMO energies and their standard deviations suggest that the energy fluctuations are similar for PNA and DNA duplexes. These HOMO energies, calculated *in vacuo*, are 1.5−2 eV below the Au work function. However, the influence of a metal electrode on the electronic state energies of adsorbed species can be substantial (~1 eV[66]), and we expect the energy offset between the Fermi level and the effective HOMO orbital energies to be significantly less than 1.5−2 eV.

Table 2. HOMO Energies (eV) and Their Standard Deviations for the GC Base Pairs Examined in the Cross-Strand, Intrastrand, and Terminal Electronic Coupling Calculations[a]

	5′ DNA		3′ DNA		PNA N-end	
	E_{HOMO}	σ	E_{HOMO}	σ	E_{HOMO}	σ
cross	−6.51	0.22	−6.55	0.21	−6.97	0.19
intra	−6.41	0.22	−6.37	0.21	−6.47	0.19
term	−6.68	0.21	−6.71	0.22	−6.56	0.18

[a]These values are computed for n = 5 chains.

We calculated the nearest-neighbor root-mean-square electronic couplings (V_{RMS}) between base pairs (INDO/S, block diagonalization method, capped bases),[32] where $V_{RMS} = \sqrt{\langle V^2 \rangle} = (1/n)\sqrt{\sum_{i=1}^{n} V_i^2}$, where $V_{RMS}^2 = \langle V \rangle^2 + \sigma^2$, σ is the standard deviation of V, and n is the number of MD snapshots used for averaging. Table 3 shows the calculated

Table 3. V_{RMS} Values of GC-GC Cross-Strand (V_C), GC-GC Intrastrand (V_I), and Terminal AT-GC Coupling (V_T) in Electronvolts[a]

	5′ DNA	3′ DNA	PNA N-end
V_T	0.011	0.017	0.047
V_I	0.087	0.071	0.120
V_C	0.006	0.012	0.002
V_C^{SE}	0.001	0.005	0.017

[a]The cross-strand GC-GC couplings for the superexchange pathway (V_C^{SE}) are also shown.

V_{RMS} values. Table 3 reports the calculated electronic couplings of the terminal AT base pairs with their nearest GC pair (V_T) for each of the three duplex types. These calculations indicate a nearly 3-fold increase in V_T for N-terminal PNA compared to the corresponding couplings in the DNA duplexes. Table 3 also shows that the N-linker PNA duplex intrastrand couplings (V_I) are larger than the values found for the DNA counterpart. The increases in the couplings, V_I and V_T, for PNA versus DNA are consistent with the larger molecular conductances that are observed experimentally. The cross-strand coupling (V_C) also affects the conductance, and earlier work[30] showed that it affects the even−odd oscillations which are discussed next. A description of how these computed electronic coupling values are linked to the conductance measurements follows this subsection.

The direct cross-strand couplings V_C of the N-linked PNA and 5′-linked DNA are both small compared to the other couplings, presumably because of the small overlaps between the G bases on the two strands (Figure S7). Thus, we examined how these values compared with coupling obtained from a superexchange pathway involving three nucleobases, V_C^{SE} (Table 3). MD simulations show that the geometrical parameters of PNA produce larger G-C π-overlaps in the cross-strand region and, as a consequence, stronger π-couplings compared to the case in DNA (see Figure S8). The strong π-interaction between the stacked GC nucleobases in PNA provides a superexchange pathway for charge transfer. The cross-strand coupling, V_C^{SE}, for the guanine-cytosine-guanine superexchange pathway was calculated for selected snapshots

https://doi.org/10.1021/acs.biochem.1c00072
Biochemistry 2021, 60, 1368−1378

taken every 5 ns with density functional theory to describe hydrogen bonding interactions (M11/ma-def2-TZVPP, block diagonalization, capped bases).[58,67] $V_C^{SE} = \frac{V_{G5\text{-}C6}V_{G6\text{-}C6}}{\Delta E}$, where the subscripts indicate the nucleobase and the position in the n = 5 duplex (see Figure S10) and ΔE is the difference in energy between guanine and cytosine localized states, which is close to 0.7 eV.[68,69] V_C^{SE} values, which are the RMS couplings, are included in Table 3. V_C^{SE} is larger than the RMS V_C values for only PNA, suggesting that the superexchange contribution to the cross-strand coupling is more relevant to the transport mechanism in PNA than in DNA, and we will address the implications for charge transport below.

In addition to differences in coupling pathways for PNA and DNA, the MD simulations reveal structural differences among the duplexes that can affect the electrode−molecule electronic couplings (γ_L and γ_R). Recall that V_T and γ_L and γ_R determine the electronic coupling interactions near the chain ends. The orientation of the terminal AT base pair, which contains the amine groups that bind to the Au electrodes, with respect to the first GC base pair of the G-block (see Figure 1) appears to be different in the PNA junctions and in the DNA duplexes. In particular, the DNA terminal base pairs exhibit larger structural fluctuations than in PNA, which leads to "fraying" of the duplex in the absence of the distance constraint described above. In addition, the increased rigidity of the PNA nucleobases, which correlates with enhanced $\pi-\pi$ stacking interactions, likely contributes to establishing strong contacts with the leads and increasing the conductance.

PNA versus DNA Conductance. The average experimentally measured single-molecule length-dependent conductance for the high-conductance mode of each duplex is shown in Figure 4. For the N-to-N linked PNA, the average conductance of the highest-conductance mode is ∼3 × 10^{-2} G/G_0 (where G_0 is the quantum of conductance). The average conductances for the PNA duplexes are an order of magnitude larger (or more) than for DNA duplexes of the same length. Figure 4b shows the mean conductance value obtained from the PNA conductance histograms, which are 3−5 times larger than the literature conductance values reported for 3′ DNA. In addition to the PNA conductances, the conductances for the first few (n = 3, 4, and 5) 3′- and 5′-linked G-block DNA duplexes were measured in this study and are plotted as filled symbols in Figure 4. The measurements performed here are in good agreement with those reported by Tao and co-workers (empty symbols) and also display the even−odd oscillation.[30] Note that the increased conductance in PNA compared to DNA is consistent with earlier findings for mixed PNA sequences,[29,36] although the details of the mechanism for the large PNA conductance may be different.

The G-block PNA molecules show a significantly higher conductance (2−4% of G_0) than is typically found for molecules of a comparable length, ∼3−5 nm.[70] For example, molecules that display conductances on the order of a few percent of G_0 are typically the size of a single aromatic ring, e.g., benzenedithiol and benzenediamine. Two key factors influencing the molecular conductance in a junction are the electrode−molecule linker group and the molecule's electronic structure. The linker group can have order(s) of magnitude effects on the measured conductance.[70,71] The amine linkers for the PNA and DNA duplexes used in this study couple the aromatic stack of the duplex more strongly to the electrode than do the backbone-based thiol linkers used in earlier studies.[72] The electronic structure of the mediating molecule, e.g., saturated versus unsaturated, is known to have a strong influence on the molecular conductance, as well.[68] However, molecules with highly conjugated electronic structures, such as oligo(phenylene-vinylenes) and oligophenylethynylenes, show conductances in the range of ≤10^{-3} G_0 if they are a few nanometers in length.[70,73] The length dependence of the molecular conductance through a homologous series of molecules is often characterized using an exponential decay as a function of length L, i.e., $\exp(-\beta L)$.[74] Conjugated molecules show a much weaker decay with distance (smaller β value) than do saturated systems. Both the shallow dependence of the PNA conductances on length and the high conductance values are consistent with transport mediated by extended π-systems.

The observation that the molecular conductances of G-block PNA duplexes are 10−20 times higher than those of the corresponding 5′ DNA duplexes with the π-stacked linkers is consistent with previous observations. Bruot et al.[72] compared the molecular conductance through 5′A$(CG)_n$T3′ (n = 2−12) DNA duplexes consisting of thiol linker groups connecting to the nucleic acid backbone with duplexes of the identical nucleobase sequence that have amine linkers bonded directly to the base stack. They found that the conductance was 10−20 times higher for the π-stack linker than for the backbone linker for otherwise identical DNA duplexes. In earlier studies, we compared the molecular conductance of PNA duplexes to that of DNA duplexes with thiol linker groups on the nucleic acid backbone. In those cases, the PNA displayed a molecular conductance that was ∼20 times higher than that of the DNA.[29,36] The high conductances measured for the PNA duplexes in this study are consistent with these earlier findings. The combined effects of the amine/thymine-based linker group and the high electronic coupling through the G-block stack are responsible for the high conductances reported here (*vide infra*).

Molecular Orbital Interpretation of Conductance Oscillations. The N-to-N linked PNA duplexes show a 1−2-order of magnitude increase in the molecular conductance compared to the values for the corresponding 5′-linked DNAs. This increase in conductance is consistent with the findings for mixed sequence DNA and PNA duplexes reported previously.[29,36] Conductance oscillations observed previously in the 5′-linked and 3′-linked DNA systems are barely evident for the PNA duplexes. The decreased amplitude of the even−odd oscillations with G-block length is explained by the larger cross-strand coupling and electrode−molecule couplings in PNA. We first discuss the cross-strand coupling effect and then examine the influence of electrode−molecule coupling on the conductance oscillations.

In earlier studies, conductance oscillations as a function of length in G-block DNA duplexes (see Figure 4) were explained by an electronic energy effect that arises in finite length periodic structures.[30,75,76] Odd length G-blocks possess a "midband" localized orbital with an energy near the Fermi level of the gold electrode, approximately equal to the energy of a G monomer.[30] This length-independent near degeneracy was proposed to strengthen coherent charge transport for odd length chains by providing a flickering resonance coupling pathway across the entire duplex.[30] In contrast, the orbital energies for even length G-blocks are offset from the "midband" position (Figure 5) and are unlikely to form flickering resonance coupling pathways across the structures.

https://doi.org/10.1021/acs.biochem.1c00072
Biochemistry 2021, 60, 1368−1378

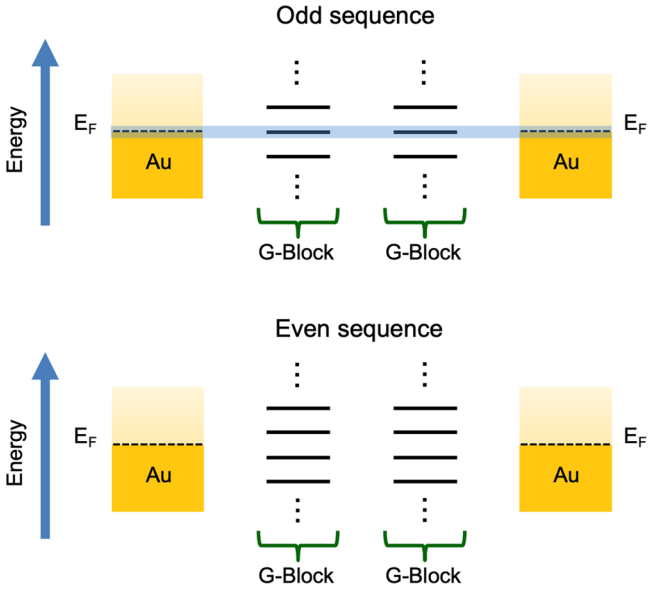

Figure 5. Molecular orbital energy picture of nucleic acid duplexes with a weak cross-strand coupling. Flickering resonance energy level alignment for odd length sequences (top). Each G-block possesses a midband orbital in resonance with the Fermi level of the electrodes. Energy level alignment for even sequences (bottom). A midband state in resonance with the Fermi level of the electrodes is absent.

This picture accounts for the oscillations of conductance with length, as shown in Figure 4.

Figure 4 shows that the amplitude of the conductance oscillations decrease through the three duplex types as the overall conductance of the duplex increases. For example, the oscillations in conductance are substantially less pronounced when the molecular linkers are positioned at the 3′ termini of DNA, as compared to the 5′ termini, and the corresponding molecular conductance of the 3′ species is observed to be larger. The decrease in the amplitude of the oscillations of conductance, and the overall increase in conductance in DNA, was attributed to geometric differences of the base pairs at the cross-stand position in the two cases (Figures S7 and S8), which causes a change in the cross-strand coupling.[30] Intriguingly, a large cross-strand GC-GC coupling at the molecule's center reduces the likelihood of forming a fully delocalized (resonant) state across the G-blocks and the electrodes (*vide infra*).[77]

As a rule of thumb, the number of G bases over which the hole can delocalize at room temperature can reach five.[30,78] When the cross-strand coupling is weak, as in 5′ DNA, the dominant position for the delocalized hole is across the n guanines that form each of the separate G-blocks, forming two domains. Thermal fluctuations can bring these two domains into resonance, i.e., flickering resonance, and form a fully delocalized state across the entire duplex[37] (Figure 6). Because the odd length G-blocks have resonant states near the Fermi level, and the even length G-blocks do not, a strong modulation of the conductance with the G-block length is predicted to manifest. As the cross-strand coupling increases, delocalization can occur among G nucleobases of the two blocks, and this leads to a lower statistical weight for configurations that have the hole delocalized over each of the G-blocks. The growth in the number of configurations with delocalized domains leads to a higher overall conductance. The

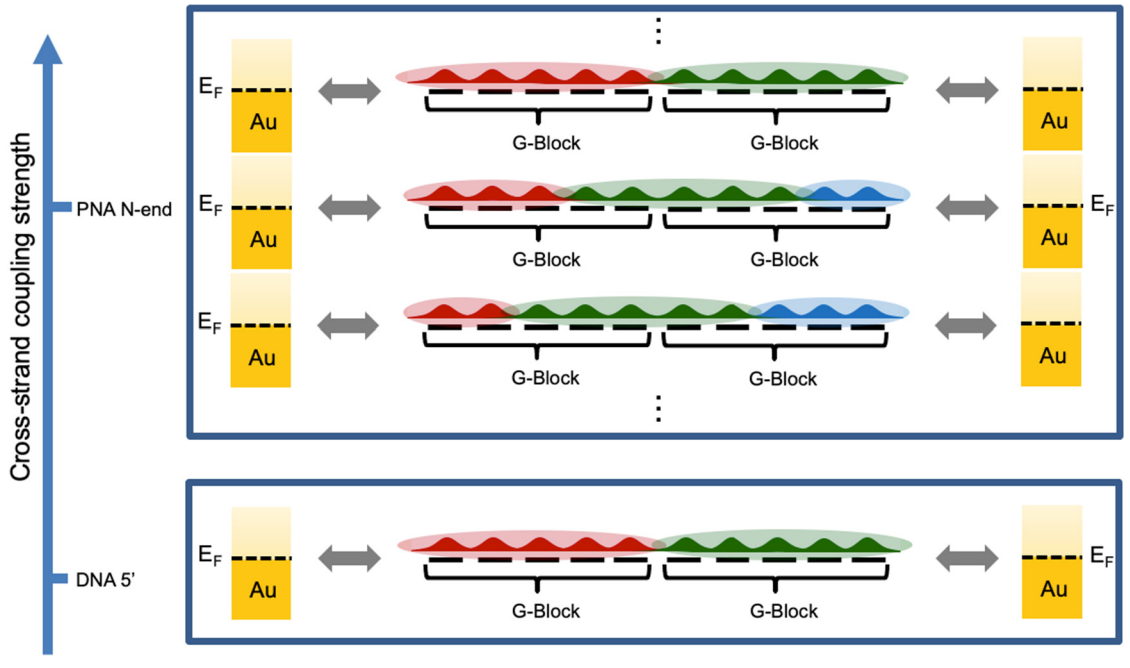

Figure 6. Model describing the delocalized islands across two G-blocks, each with $n = 5$. The maximum number of G residues over which the hole can delocalize can reach five (each color represents a delocalized block of orbitals).[30,78] Regime with a strong cross-strand coupling (top). The strong cross-strand coupling allows the five-base pair delocalization to occur anywhere across the entire ten-base sequence of the G-blocks (e.g., the green block can be delocalized across the two strands). Therefore, the carrier position in PNA is less constrained than in DNA. For the sake of illustration, three possible configurations that support delocalization are shown (many others are possible). Regime in which the coherent channel with the hole delocalized over each G-block contributes significantly to the conductance (bottom). This coherent channel is absent in even length sequences (see Figure 5).[30,75] The weak cross-strand coupling pins the carrier delocalization on one of the G-blocks. The odd length G-block sequences are near resonant with the Fermi level of the leads and create a delocalized state for coherent transport.

https://doi.org/10.1021/acs.biochem.1c00072
Biochemistry 2021, 60, 1368−1378

decreased statistical importance of the configuration with the extended G-block delocalization manifests as a decrease in the amplitude of the even−odd length conductance oscillations. Overall, the conductance is limited by the squared coupling between these domains and by the molecule−lead interaction strengths. The observation that the conductance increases from 5′ DNA to 3′ DNA, and increases further as the backbone is switched to PNA, is consistent with growth in the number and size of the cross-strand delocalization domains and their importance for charge transport (switching from 5′ to 3′ increases the cross-strand coupling 3−4-fold, and switching to PNA increases the coupling by almost another 2-fold).

Figure 6 illustrates this mechanistic explanation for the change in conductance and in the even−odd effect for 5′ DNA and PNA. The bottom panel illustrates the mechanistic picture described in our prior analysis of the even and odd effects on the 5′-linked DNA conductance.[30] In this structure, the weaker cross-strand coupling in the 5′ structure (compared to that in the 3′ structure) leads to delocalization of orbitals on each of the two separated G blocks. Formation of a transient structure with extended delocalization only requires bringing these two blocks into resonance with each other and with the electrodes. This was illustrated in Figure 5 for the case of odd length (n = 3) and even length (n = 4) chains to underscore how the energies of the G-block states are offset from the Fermi level of the electrodes. The dependence of the energy mismatch on whether n is even or n is odd, and the promotion of delocalization across each G-block by the weak cross-strand coupling, leads to a strong even−odd conductance effect.

The top panel in Figure 6 explains the mechanistic picture for the case in which the cross-strand coupling is large (comparable to intrastrand GC-GC couplings). In this case, many possible delocalized islands of approximately five or fewer Gs may form in the structure. Indeed, in this regime, the likelihood of forming a delocalized state spread over the entire length of each G-block is diminished because of the increase in the overall number of other possible configurations that support delocalization, as illustrated by the two additional configurations shown in the top panel of Figure 6. Although this effect creates delocalized islands with more than one energy mismatch (so that multiple level matchings are required to delocalize over the entire molecule), many more configurations that display these delocalized islands manifest and provide many more flickering resonance conductance pathways in PNA, which leads to an overall increase in its conductance.

Our theoretical analysis (Table 3 and discussion) suggests that the electrode−molecule couplings for the PNA duplexes are stronger than in the 3′-linked and 5′-linked DNA. This feature is not included in the diagrams of Figure 6 for the sake of simplicity. A stronger electrode−molecule coupling is expected to produce a stronger mixing between the gold and the G-blocks of PNA compared to DNA. The stronger molecule−lead coupling is expected to further enhance the conductance of PNA. This prediction is consistent with the observed higher conductance in PNA and softer even−odd effect compared to that in DNA. We note that strong molecule−lead interactions can perturb the "band structure" for each G-block and will shift the energy of the midband state that appears for odd length chains. The effect of the strong molecule−lead coupling can break the degeneracy between delocalized hole states in each G-block and dampen the conductance oscillations in PNA compared to the case in 5′ DNA. This scenario was explored in detail by Segal et al., who showed that strong molecule−lead hybridization can indeed cause the even−odd effects to vanish.[75]

CONCLUSIONS

The transport of charge through nucleic acids can access coherent, incoherent, and flickering resonance mechanisms. The experimental and theoretical studies reported here find that structural differences in the duplex backbone with the same base sequences can produce order of magnitude changes in molecular conductances and can strongly influence how coherence manifests for single-molecule PNA and DNA junctions. For PNA duplexes, a conductance value of 0.03 G_0 was found with 14 base pairs (∼50 Å). PNA also has a high-mode conductance that is ≤30 times larger than that of DNA, and the conductance decreases monotonically with duplex length. The corresponding DNA structures show a striking conductance oscillation. The nearly monotonic and weak (<2-fold for distances from ∼2 to 5 nm) change in conductance with duplex length that is found in PNA indicates an extremely low molecular resistance, in strong contrast with that for the 5′-linked DNA duplexes. The overall conductance in 5′ DNA changes by only 2-fold between the n = 3 and n = 8 G-block pairs. The even−odd conductance oscillations in 5′ DNA with G-block length can be up to 4-fold, and the average conductance in 5′ DNA is 1−2 orders of magnitude lower than in PNA. Despite these dramatic differences in the experimental conductances and their length dependences, the flickering resonance transport mechanism provides a consistent explanation for the observed behavior.

Theoretical analysis shows that the PNA and DNA G-block structures studied here have similar structural flexibility, base energy fluctuations, and base−base electronic interactions. The main differences between the PNA and DNA duplexes appear to be rooted in (1) differences in the molecule−electrode interaction strength and (2) differences in the base−base interactions in the cross-strand region, which arise from differences in geometry between duplex PNA and DNA. The stronger cross-strand and molecule−lead couplings in PNA lead to higher conductance than in DNA. As such, the characteristics of cross-strand, intrastrand, and molecule−lead couplings collectively influence the contribution of competing coupling pathways to the conductance. The mechanistic origin of the even−odd conductance effect found in the DNA is consistent with that reported previously,[30] which showed that cross-strand interactions in the center of the duplex tip the balance among mechanisms. In contrast to earlier studies, the findings reported here indicate that the conductance mechanism is also influenced by the strength of the nucleic acid−electrode interactions. Growing the electrode molecule or the block-to-block couplings is expected to reduce the statistical importance of delocalized states spread across just one G-block, leads to a decrease in the even−odd length conductance oscillations with length, and produces an overall increase in the molecular conductance. Future work should explore the effects of the molecule−lead coupling strength on conductance; for example, one can vary the aliphatic chain length of the amine linkers or modify the electrode's Fermi level to realize this goal. Detailed theoretical studies to assess the molecule−lead interactions[79] would also be incisive.

https://doi.org/10.1021/acs.biochem.1c00072
Biochemistry 2021, 60, 1368−1378

■ ASSOCIATED CONTENT

Supporting Information

The Supporting Information is available free of charge at https://pubs.acs.org/doi/10.1021/acs.biochem.1c00072.

A description of control experiments for the STM break junction measurements, details of DNA conductance measurements reported in Figures 3 and 4, detailed MD procedures, RMSD plots, helical parameters, analysis of average structures from the MD production runs, HOMO energies of each base pair, and details of fitting of data to eq 1 (PDF)

■ AUTHOR INFORMATION

Corresponding Authors

Peng Zhang − *Department of Chemistry, Duke University, Durham, North Carolina 27708, United States*; Email: peng.zhang@duke.edu

David N. Beratan − *Department of Chemistry, Department of Physics, and Department of Biochemistry, Duke University, Durham, North Carolina 27708, United States*; orcid.org/0000-0003-4758-8676; Email: david.beratan@duke.edu

David H. Waldeck − *Department of Chemistry, University of Pittsburgh, Pittsburgh, Pennsylvania 15260, United States*; orcid.org/0000-0003-2982-0929; Email: dave@pitt.edu

Authors

Jesús Valdiviezo − *Department of Chemistry, Duke University, Durham, North Carolina 27708, United States*

Caleb Clever − *Department of Chemistry, University of Pittsburgh, Pittsburgh, Pennsylvania 15260, United States*

Edward Beall − *Department of Chemistry, University of Pittsburgh, Pittsburgh, Pennsylvania 15260, United States*

Alexander Pearse − *Department of Chemistry, Carnegie Mellon University, Pittsburgh, Pennsylvania 15213, United States*

Yookyung Bae − *Department of Chemistry, Carnegie Mellon University, Pittsburgh, Pennsylvania 15213, United States*

Catalina Achim − *Department of Chemistry, Carnegie Mellon University, Pittsburgh, Pennsylvania 15213, United States*; orcid.org/0000-0001-5420-4656

Complete contact information is available at: https://pubs.acs.org/10.1021/acs.biochem.1c00072

Author Contributions

[#]J.V. and C.C. contributed equally to this work.

Funding

This material is based upon work supported by the National Science Foundation (Grants 1412030 and 1900078 to D.H.W., 1413202 to C.A., and 1925690 to J.V., P.Z., and D.N.B.). E.B. acknowledges a fellowship from the Pittsburgh Quantum Institute during part of this work. J.V. acknowledges support of a Fulbright-García Robles Scholarship.

Notes

The authors declare no competing financial interest.

■ ACKNOWLEDGMENTS

J.V. is grateful to Dr. Yuqi Zhang and Prof. Julio L. Palma for helpful discussions.

■ REFERENCES

(1) Genereux, J. C., and Barton, J. K. (2010) Mechanisms for DNA charge transport. *Chem. Rev. 110* (3), 1642−1662.

(2) Lewis, F. D., Young, R. M., and Wasielewski, M. R. (2018) Tracking photoinduced charge separation in DNA: from start to finish. *Acc. Chem. Res. 51* (8), 1746−1754.

(3) Lewis, F. D., Wu, T., Zhang, Y., Letsinger, R. L., Greenfield, S. R., and Wasielewski, M. R. (1997) Distance-dependent electron transfer in DNA hairpins. *Science 277* (5326), 673−676.

(4) Fink, H.-W., and Schönenberger, C. (1999) Electrical conduction through DNA molecules. *Nature 398* (6726), 407−410.

(5) Kelley, S. O., Jackson, N. M., Hill, M. G., and Barton, J. K. (1999) Long-range electron transfer through DNA films. *Angew. Chem. Int. Ed. 38* (7), 941−945.

(6) Giese, B., Amaudrut, J., Köhler, A.-K., Spormann, M., and Wessely, S. (2001) Direct observation of hole transfer through DNA by hopping between adenine bases and by tunnelling. *Nature 412* (6844), 318−320.

(7) Xu, B., Zhang, P., Li, X., and Tao, N. (2004) Direct conductance measurement of single DNA molecules in aqueous solution. *Nano Lett. 4* (6), 1105−1108.

(8) Risser, S. M., Beratan, D. N., and Meade, T. J. (1993) Electron transfer in DNA: predictions of exponential growth and decay of coupling with donor-acceptor distance. *J. Am. Chem. Soc. 115* (6), 2508−2510.

(9) Jortner, J., Bixon, M., Langenbacher, T., and Michel-Beyerle, M. E. (1998) Charge transfer and transport in DNA. *Proc. Natl. Acad. Sci. U. S. A. 95* (22), 12759−12765.

(10) Renaud, N., Berlin, Y. A., Lewis, F. D., and Ratner, M. A. (2013) Between superexchange and hopping: An intermediate charge-transfer mechanism in poly (A)-poly (T) DNA hairpins. *J. Am. Chem. Soc. 135* (10), 3953−3963.

(11) Beratan, D. N. (2019) Why are DNA and protein electron transfer so different? *Annu. Rev. Phys. Chem. 70*, 71−97.

(12) Beratan, D. N., Liu, C., Migliore, A., Polizzi, N. F., Skourtis, S. S., Zhang, P., and Zhang, Y. (2015) Charge transfer in dynamical biosystems, or the treachery of (static) images. *Acc. Chem. Res. 48* (2), 474−481.

(13) Korol, R., and Segal, D. (2018) From exhaustive simulations to key principles in DNA nanoelectronics. *J. Phys. Chem. C 122* (8), 4206−4216.

(14) Beratan, D. N., Priyadarshy, S., and Risser, S. M. (1997) DNA: insulator or wire? *Chem. Biol. 4* (1), 3−8.

(15) Priyadarshy, S., Risser, S., and Beratan, D. (1996) DNA is not a molecular wire: protein-like electron-transfer predicted for an extended π-electron system. *J. Phys. Chem. 100* (44), 17678−17682.

(16) Teo, R. D., Rousseau, B. J., Smithwick, E. R., Di Felice, R., Beratan, D. N., and Migliore, A. (2019) Charge transfer between [4Fe4S] proteins and DNA is unidirectional: Implications for biomolecular signaling. *Chem. 5* (1), 122−137.

(17) Kilgour, M., and Segal, D. (2015) Charge transport in molecular junctions: From tunneling to hopping with the probe technique. *J. Chem. Phys. 143* (2), No. 024111.

(18) Berlin, Y. A., Burin, A. L., and Ratner, M. A. (2001) Charge hopping in DNA. *J. Am. Chem. Soc. 123* (2), 260−268.

(19) Berlin, Y. A., Kurnikov, I. V., Beratan, D., Ratner, M. A., and Burin, A. L. (2004) DNA electron transfer processes: Some theoretical notions. In *Long-Range Charge Transfer in DNA II* (Schuster, G. B., Ed.) pp 1−36, Springer, Berlin.

(20) Venkatramani, R., Davis, K. L., Wierzbinski, E., Bezer, S., Balaeff, A., Keinan, S., Paul, A., Kocsis, L., Beratan, D. N., Achim, C., and Waldeck, D. H. (2011) Evidence for a near-resonant charge transfer mechanism for double-stranded peptide nucleic acid. *J. Am. Chem. Soc. 133* (1), 62−72.

(21) Xiang, L., Palma, J. L., Bruot, C., Mujica, V., Ratner, M. A., and Tao, N. (2015) Intermediate tunnelling−hopping regime in DNA charge transport. *Nat. Chem. 7* (3), 221−226.

(22) Michaeli, K., Beratan, D. N., Waldeck, D. H., and Naaman, R. (2019) Voltage-induced long-range coherent electron transfer

through organic molecules. *Proc. Natl. Acad. Sci. U. S. A. 116* (13), 5931−5936.
(23) Buttiker, M. (1988) Coherent and sequential tunneling in series barriers. *IBM J. Res. Dev. 32* (1), 63−75.
(24) Di Felice, R., Calzolari, A., Molinari, E., and Garbesi, A. (2001) Ab initio study of model guanine assemblies: The role of $\pi-\pi$ coupling and band transport. *Phys. Rev. B: Condens. Matter Mater. Phys. 65* (4), No. 045104.
(25) Livshits, G. I., Stern, A., Rotem, D., Borovok, N., Eidelshtein, G., Migliore, A., Penzo, E., Wind, S. J., Di Felice, R., Skourtis, S. S., et al. (2014) Long-range charge transport in single G-quadruplex DNA molecules. *Nat. Nanotechnol. 9* (12), 1040−1046.
(26) Wierzbinski, E., Venkatramani, R., Davis, K. L., Bezer, S., Kong, J., Xing, Y., Borguet, E., Achim, C., Beratan, D. N., and Waldeck, D. H. (2013) The single-molecule conductance and electrochemical electron-transfer rate are related by a power law. *ACS Nano 7* (6), 5391−5401.
(27) Wolak, M. u. A., Balaeff, A., Gutmann, S., Helmrich, H. J., Vosloo, R., Beerbom, M. M., Wierzbinski, E., Waldeck, D. H., Bezer, S., Achim, C., et al. (2011) Electronic structure of self-assembled peptide nucleic acid thin films. *J. Phys. Chem. C 115* (34), 17123−17135.
(28) Paul, A., Bezer, S., Venkatramani, R., Kocsis, L., Wierzbinski, E., Balaeff, A., Keinan, S., Beratan, D. N., Achim, C., and Waldeck, D. H. (2009) Role of nucleobase energetics and nucleobase interactions in single-stranded peptide nucleic acid charge transfer. *J. Am. Chem. Soc. 131* (18), 6498−6507.
(29) Beall, E., Sargun, A., Ulku, S., Bae, Y., Wierzbinski, E., Clever, C., Waldeck, D. H., and Achim, C. (2018) Molecular conductance of nicked nucleic acid duplexes. *J. Phys. Chem. C 122* (13), 7533−7540.
(30) Liu, C., Xiang, L., Zhang, Y., Zhang, P., Beratan, D. N., Li, Y., and Tao, N. (2016) Engineering nanometre-scale coherence in soft matter. *Nat. Chem. 8* (10), 941−945.
(31) Šponer, J., Leszczyński, J., and Hobza, P. (1996) Nature of nucleic acid− base stacking: nonempirical ab initio and empirical potential characterization of 10 stacked base dimers. Comparison of stacked and H-bonded base pairs. *J. Phys. Chem. 100* (13), 5590−5596.
(32) Voityuk, A. A. (2008) Electronic couplings and on-site energies for hole transfer in DNA: Systematic quantum mechanical/molecular dynamic study. *J. Chem. Phys. 128* (11), No. 115101.
(33) Hatcher, E., Balaeff, A., Keinan, S., Venkatramani, R., and Beratan, D. N. (2008) PNA versus DNA: Effects of structural fluctuations on electronic structure and hole-transport mechanisms. *J. Am. Chem. Soc. 130* (35), 11752−11761.
(34) Venkatramani, R., Keinan, S., Balaeff, A., and Beratan, D. N. (2011) Nucleic acid charge transfer: black, white and gray. *Coord. Chem. Rev. 255* (7−8), 635−648.
(35) Wierzbinski, E., de Leon, A., Yin, X., Balaeff, A., Davis, K. L., Reppireddy, S., Venkatramani, R., Keinan, S., Ly, D. H., Madrid, M., et al. (2012) Effect of backbone flexibility on charge transfer rates in peptide nucleic acid duplexes. *J. Am. Chem. Soc. 134* (22), 9335−9342.
(36) Beall, E., Ulku, S., Liu, C., Wierzbinski, E., Zhang, Y., Bae, Y., Zhang, P., Achim, C., Beratan, D. N., and Waldeck, D. H. (2017) Effects of the backbone and chemical linker on the molecular conductance of nucleic acid duplexes. *J. Am. Chem. Soc. 139* (19), 6726−6735.
(37) Zhang, Y., Liu, C., Balaeff, A., Skourtis, S. S., and Beratan, D. N. (2014) Biological charge transfer via flickering resonance. *Proc. Natl. Acad. Sci. U. S. A. 111* (28), 10049−10054.
(38) Egholm, M., Buchardt, O., Christensen, L., Behrens, C., Freier, S. M., Driver, D. A., Berg, R. H., Kim, S. K., Norden, B., and Nielsen, P. E. (1993) PNA hybridizes to complementary oligonucleotides obeying the Watson−Crick hydrogen-bonding rules. *Nature 365* (6446), 566−568.
(39) Xu, B., and Tao, N. J. (2003) Measurement of single-molecule resistance by repeated formation of molecular junctions. *Science 301* (5637), 1221−1223.
(40) Beall, E., Yin, X., Waldeck, D. H., and Wierzbinski, E. (2015) A scanning tunneling microscope break junction method with continuous bias modulation. *Nanoscale 7* (36), 14965−14973.
(41) Van Wees, B., Van Houten, H., Beenakker, C., Williamson, J. G., Kouwenhoven, L., Van der Marel, D., and Foxon, C. (1988) Quantized conductance of point contacts in a two-dimensional electron gas. *Phys. Rev. Lett. 60* (9), 848.
(42) Afsari, S., Li, Z., and Borguet, E. (2014) Orientation-Controlled Single-Molecule Junctions. *Angew. Chem. Int. Ed. 53* (37), 9771−9774.
(43) Komoto, Y., Fujii, S., Nishino, T., and Kiguchi, M. (2015) High electronic couplings of single mesitylene molecular junctions. *Beilstein J. Nanotechnol. 6* (1), 2431−2437.
(44) Hanwell, M. D., Curtis, D. E., Lonie, D. C., Vandermeersch, T., Zurek, E., and Hutchison, G. R. (2012) Avogadro: an advanced semantic chemical editor, visualization, and analysis platform. *J. Cheminf. 4* (1), 17.
(45) *Maestro*, release 2019-4 (2019) Schrödinger, LLC, New York.
(46) Yeh, J. I., Pohl, E., Truan, D., He, W., Sheldrick, G. M., Du, S., and Achim, C. (2010) The Crystal Structure of Non-Modified and Bipyridine-Modified PNA Duplexes. *Chem. - Eur. J. 16* (39), 11867−11875.
(47) Hart, K., Foloppe, N., Baker, C. M., Denning, E. J., Nilsson, L., and MacKerell, A. D., Jr (2012) Optimization of the CHARMM additive force field for DNA: Improved treatment of the BI/BII conformational equilibrium. *J. Chem. Theory Comput. 8* (1), 348−362.
(48) Jasiński, M., Feig, M., and Trylska, J. (2018) Improved force fields for peptide nucleic acids with optimized backbone torsion parameters. *J. Chem. Theory Comput. 14* (7), 3603−3620.
(49) Jorgensen, W. L., Chandrasekhar, J., Madura, J. D., Impey, R. W., and Klein, M. L. (1983) Comparison of simple potential functions for simulating liquid water. *J. Chem. Phys. 79* (2), 926−935.
(50) Zgarbová, M., Otyepka, M., Sponer, J., Lankas, F., and Jurečka, P. (2014) Base pair fraying in molecular dynamics simulations of DNA and RNA. *J. Chem. Theory Comput. 10* (8), 3177−3189.
(51) Phillips, J. C., Braun, R., Wang, W., Gumbart, J., Tajkhorshid, E., Villa, E., Chipot, C., Skeel, R. D., Kale, L., and Schulten, K. (2005) Scalable molecular dynamics with NAMD. *J. Comput. Chem. 26* (16), 1781−1802.
(52) Pacher, T., Cederbaum, L., and Köppel, H. (1988) Approximately diabatic states from block diagonalization of the electronic Hamiltonian. *J. Chem. Phys. 89* (12), 7367−7381.
(53) Ridley, J., and Zerner, M. (1973) An intermediate neglect of differential overlap technique for spectroscopy: pyrrole and the azines. *Theor. Chim. Acta 32* (2), 111−134.
(54) Zeng, J., Hush, N., and Reimers, J. (1996) Solvent effects on molecular and ionic spectra. 7. Modeling the absorption and electroabsorption spectra of pentaammine-ruthenium (II) pyrazine and its conjugate acid in water. *J. Am. Chem. Soc. 118* (8), 2059−2068.
(55) Voityuk, A. A. (2006) Assessment of semiempirical methods for the computation of charge transfer in DNA π-stacks. *Chem. Phys. Lett. 427* (1−3), 177−180.
(56) Kubař, T., and Elstner, M. (2008) What governs the charge transfer in DNA? The role of DNA conformation and environment. *J. Phys. Chem. B 112* (29), 8788−8798.
(57) Kubař, T., Kleinekathöfer, U., and Elstner, M. (2009) Solvent fluctuations drive the hole transfer in DNA: a mixed quantum−classical study. *J. Phys. Chem. B 113* (39), 13107−13117.
(58) Boese, A. D. (2015) Density functional theory and hydrogen bonds: are we there yet? *ChemPhysChem 16* (5), 978−985.
(59) Peverati, R., and Truhlar, D. G. (2011) Improving the accuracy of hybrid meta-GGA density functionals by range separation. *J. Phys. Chem. Lett. 2* (21), 2810−2817.
(60) Zheng, J., Xu, X., and Truhlar, D. G. (2011) Minimally augmented Karlsruhe basis sets. *Theor. Chem. Acc. 128* (3), 295−305.
(61) Frisch, M. J., Trucks, G. W., Schlegel, H. B., Scuseria, G. E., Robb, M. A., Cheeseman, J. R., Scalmani, G., Barone, V., Petersson, G. A., Nakatsuji, H., Li, X., Caricato, M., Marenich, A. V., Bloino, J.,

https://doi.org/10.1021/acs.biochem.1c00072
Biochemistry 2021, 60, 1368−1378

Janesko, B. G., Gomperts, R., Mennucci, B., Hratchian, H. P., Ortiz, J. V., Izmaylov, A. F., Sonnenberg, J. L., Williams-Young, D., Ding, F., Lipparini, F., Egidi, F., Goings, J., Peng, B., Petrone, A., Henderson, T., Ranasinghe, D., Zakrzewski, V. G., Gao, J., Rega, N., Zheng, G., Liang, W., Hada, M., Ehara, M., Toyota, K., Fukuda, R., Hasegawa, J., Ishida, M., Nakajima, T., Honda, Y., Kitao, O., Nakai, H., Vreven, T., Throssell, K., Montgomery, J. A., Jr., Peralta, J. E., Ogliaro, F., Bearpark, M. J., Heyd, J. J., Brothers, E. N., Kudin, K. N., Staroverov, V. N., Keith, T. A., Kobayashi, R., Normand, J., Raghavachari, K., Rendell, A. P., Burant, J. C., Iyengar, S. S., Tomasi, J., Cossi, M., Millam, J. M., Klene, M., Adamo, C., Cammi, R., Ochterski, J. W., Martin, R. L., Morokuma, K., Farkas, O., Foresman, J. B., and Fox, D. J. (2016) *Gaussian 16*, rev. B.01, Gaussian, Inc., Wallingford, CT.

(62) Li, C., Pobelov, I., Wandlowski, T., Bagrets, A., Arnold, A., and Evers, F. (2008) Charge transport in single Aul alkanedithiol| Au junctions: coordination geometries and conformational degrees of freedom. *J. Am. Chem. Soc. 130* (1), 318−326.

(63) Haiss, W., Martín, S., Leary, E., Zalinge, H. v., Higgins, S. J., Bouffier, L., and Nichols, R. J. (2009) Impact of junction formation method and surface roughness on single molecule conductance. *J. Phys. Chem. C 113* (14), 5823−5833.

(64) Humphrey, W., Dalke, A., and Schulten, K. (1996) VMD: visual molecular dynamics. *J. Mol. Graphics 14* (1), 33−38.

(65) Tan, B., Hodak, M., Lu, W., and Bernholc, J. (2015) Charge transport in DNA nanowires connected to carbon nanotubes. *Phys. Rev. B: Condens. Matter Mater. Phys. 92* (7), No. 075429.

(66) Neaton, J. B., Hybertsen, M. S., and Louie, S. G. (2006) Renormalization of molecular electronic levels at metal-molecule interfaces. *Phys. Rev. Lett. 97* (21), 216405.

(67) Teo, R. D., Terai, K., Migliore, A., and Beratan, D. N. (2018) Electron transfer characteristics of 2′-deoxy-2′-fluoro-arabinonucleic acid, a nucleic acid with enhanced chemical stability. *Phys. Chem. Chem. Phys. 20* (41), 26063−26067.

(68) Roca-Sanjuán, D., Rubio, M., Merchán, M., and Serrano-Andrés, L. (2006) Ab initio determination of the ionization potentials of DNA and RNA nucleobases. *J. Chem. Phys. 125* (8), No. 084302.

(69) Kawai, K., and Majima, T. (2013) Hole transfer kinetics of DNA. *Acc. Chem. Res. 46* (11), 2616−2625.

(70) Evers, F., Korytár, R., Tewari, S., and van Ruitenbeek, J. M. (2020) Advances and challenges in single-molecule electron transport. *Rev. Mod. Phys. 92* (3), No. 035001.

(71) Tivanski, A. V., He, Y., Borguet, E., Liu, H., Walker, G. C., and Waldeck, D. H. (2005) Conjugated thiol linker for enhanced electrical conduction of gold− molecule contacts. *J. Phys. Chem. B 109* (12), 5398−5402.

(72) Bruot, C., Xiang, L., Palma, J. L., and Tao, N. (2015) Effect of mechanical stretching on DNA conductance. *ACS Nano 9* (1), 88−94.

(73) Frisenda, R., Stefani, D., and van der Zant, H. S. (2018) Quantum transport through a single conjugated rigid molecule, a mechanical break junction study. *Acc. Chem. Res. 51* (6), 1359−1367.

(74) Valdiviezo, J., Rocha, P., Polakovsky, A., and Palma, J. L. (2021) Nonexponential Length Dependence of Molecular Conductance in Acene-Based Molecular Wires. *ACS Sens. 6* (2), 477−484.

(75) Kim, H., Kilgour, M., and Segal, D. (2016) Intermediate Coherent−Incoherent Charge Transport: DNA as a Case Study. *J. Phys. Chem. C 120* (42), 23951−23962.

(76) Karasch, P., Ryndyk, D. A., and Frauenheim, T. (2018) Vibronic dephasing model for coherent-to-incoherent crossover in DNA. *Phys. Rev. B: Condens. Matter Mater. Phys. 97* (19), 195401.

(77) Carey, R., Chen, L., Gu, B., and Franco, I. (2017) When can time-dependent currents be reproduced by the Landauer steady-state approximation? *J. Chem. Phys. 146* (17), 174101.

(78) Jin, Y., Ru, X., Su, N. Q., Mei, Y., Beratan, D. N., Zhang, P., and Yang, W. (2020) Revisiting the Hole Size in Double Helical DNA with Localized Orbital Scaling Corrections. *J. Phys. Chem. B 124* (16), 3428−3435.

(79) Bag, S., Biswas, T., Jain, M., and Maiti, P. K. (2020) Anisotropic Charge Transport in Nanoscale DNA Wire. *J. Phys. Chem. C 124* (31), 16763−16772.

https://doi.org/10.1021/acs.biochem.1c00072
Biochemistry 2021, 60, 1368−1378